Supplementary Information for (New Journal of Chemistry):

Self-assembly of manganese(I) based thiolato bridged dinuclear metallacycles: synthesis, characterization, cytotoxicity evaluation and CO-releasing studies

Udit Kumar,[a] Shilpa Jose,[a] Dhanaraj Divya,[a] Pitchavel Vidhyapriya,[b] Natarajan Sakthivel*[b] and Bala. Manimaran*[a]

[a] Department of Chemistry, Pondicherry University, Puducherry, 605014, India.

Email: manimaran.che@pondiuni.edu.in

[b] Department of Biotechnology, Pondicherry University, Puducherry, 605014, India.

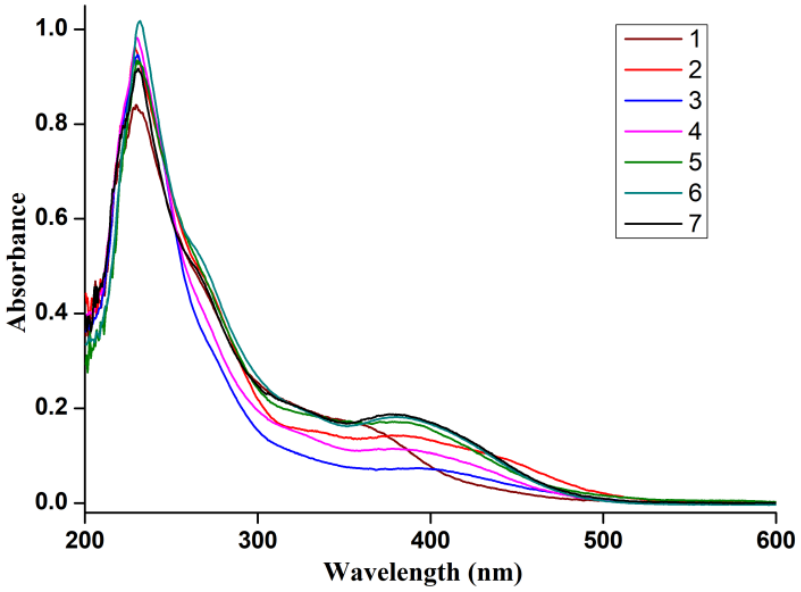

Fig. S1 Overlay plot of UV-Vis spectra of compounds **1**–**7** in CH_2Cl_2 solvent.

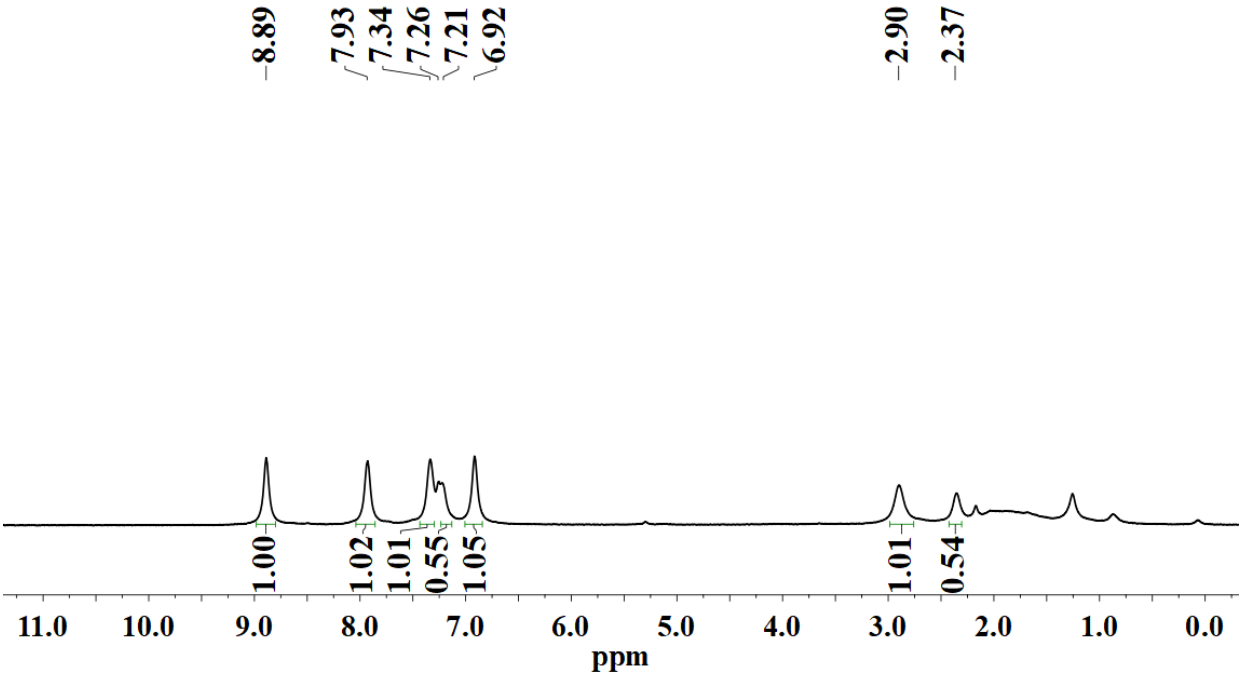

Fig. S2 ^{1}H NMR spectrum of compound **1** in $CDCl_3$.

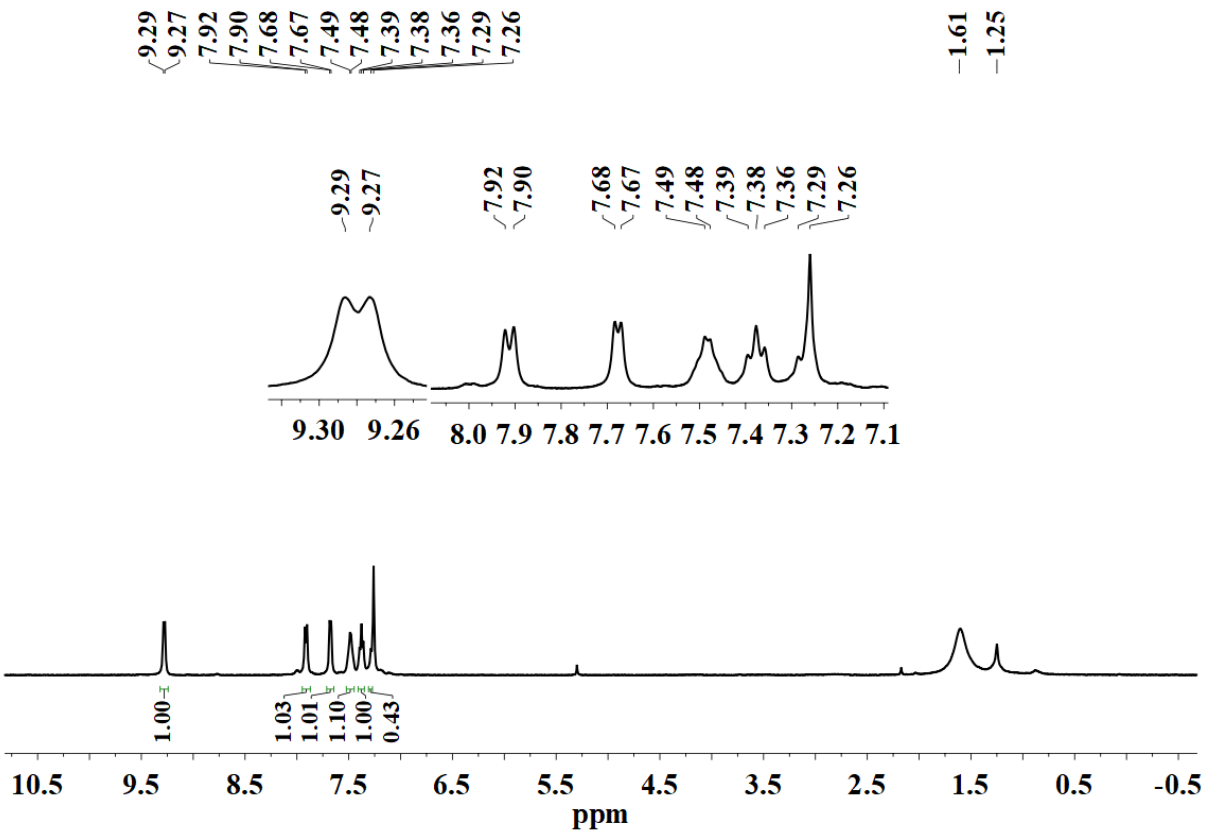

Fig. S3 ^{1}H NMR spectrum of compound **2** in $CDCl_3$.

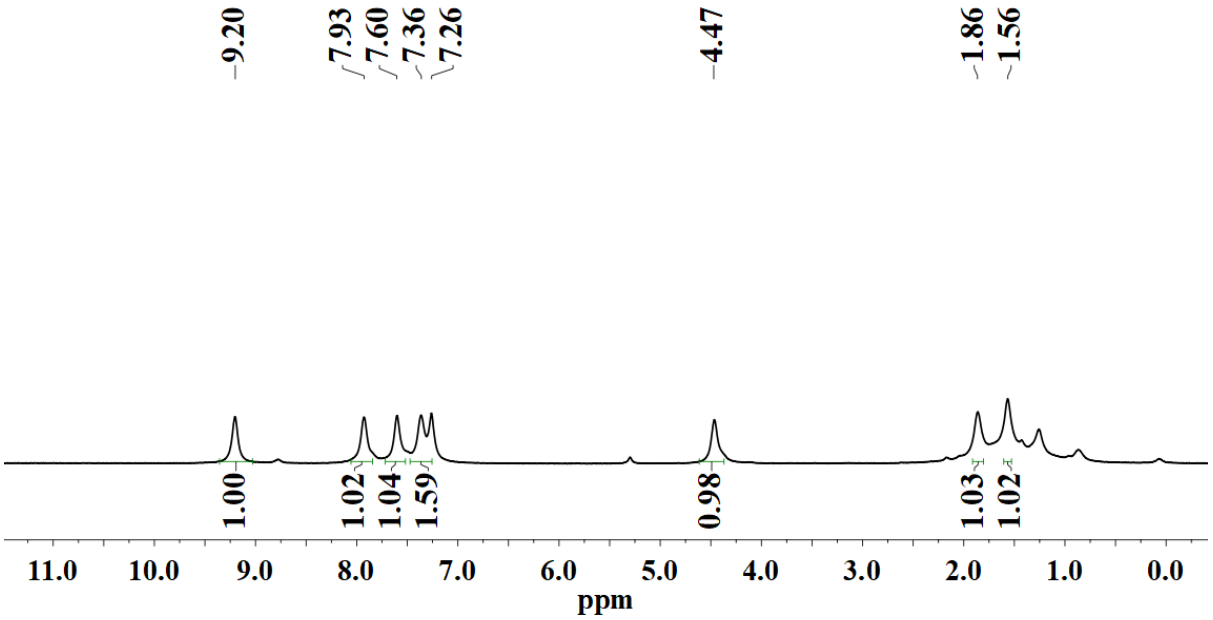

Fig. S4 ^{1}H NMR spectrum of compound **5** in $CDCl_3$.

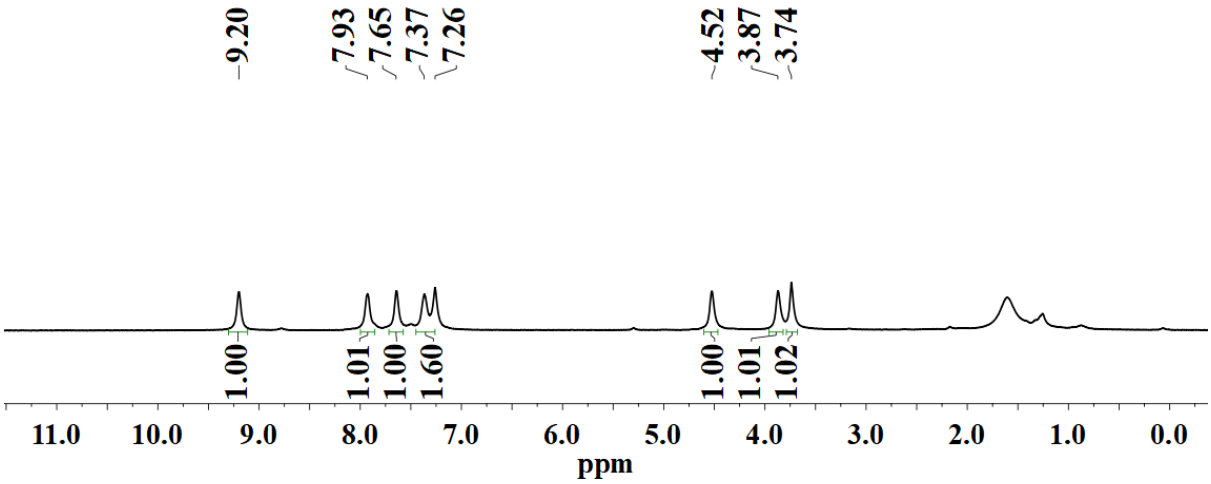

Fig. S5 ^{1}H NMR spectrum of compound **7** in $CDCl_3$.

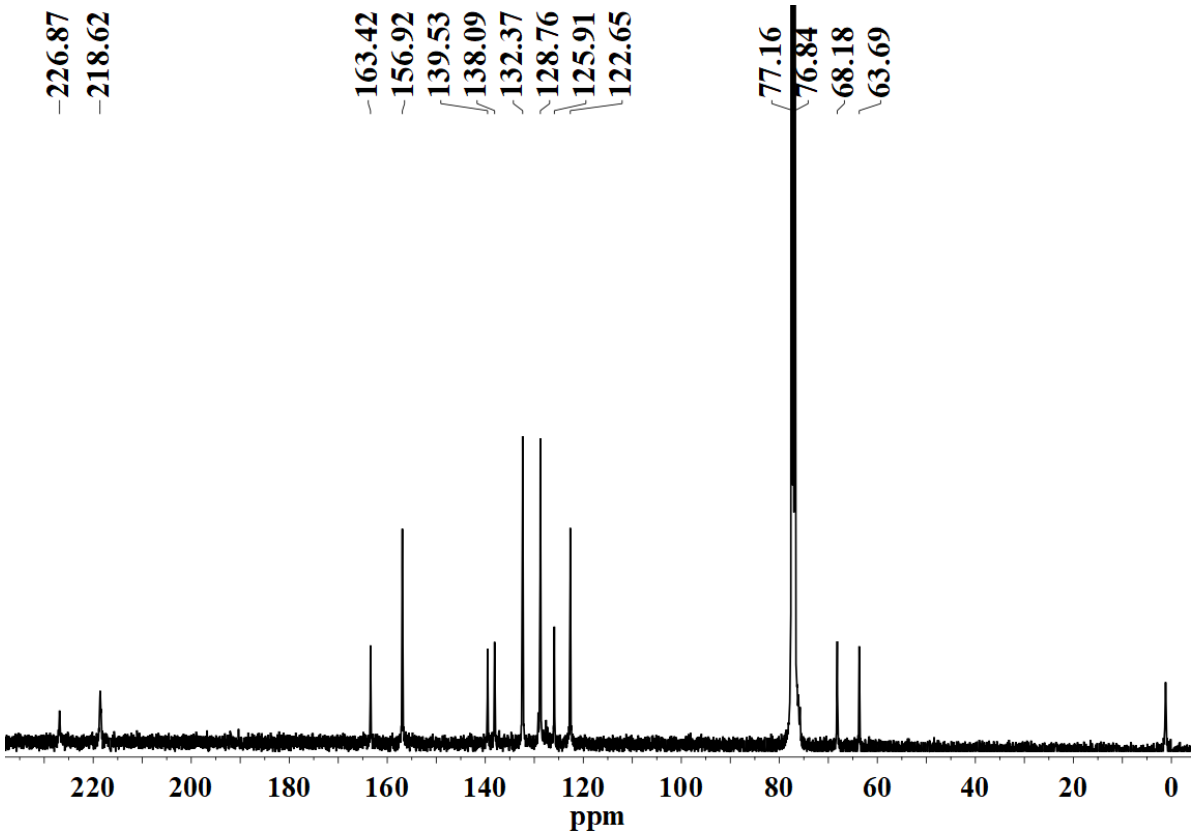

Fig. S6 ^{13}C NMR spectrum of compound **6** in $CDCl_3$.

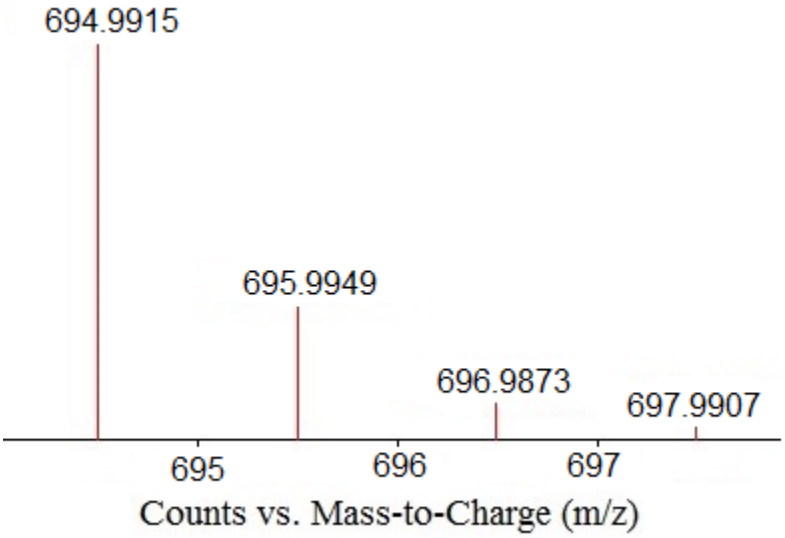

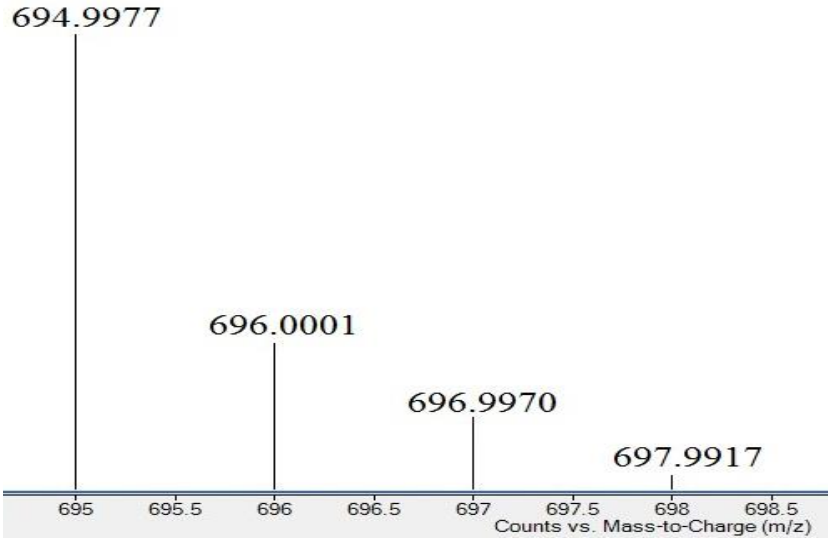

Fig. S7 ESI-MS experimental (bottom) and theoretical (top) isotopic distribution patterns of $[\{(CO)_3Mn(\mu\text{-}SC_6H_5)_2Mn(CO)_3\}(\mu\text{-bpp})]$ (**1**): $[M+H]^+$.

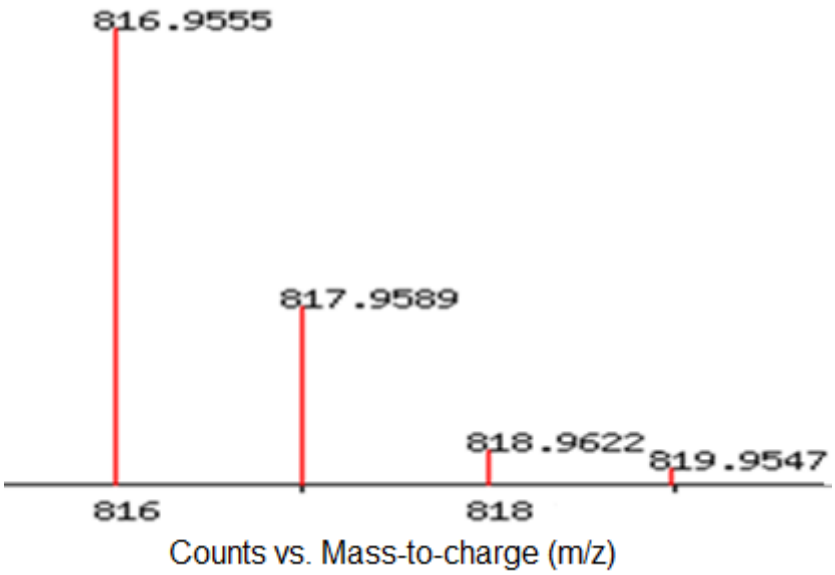

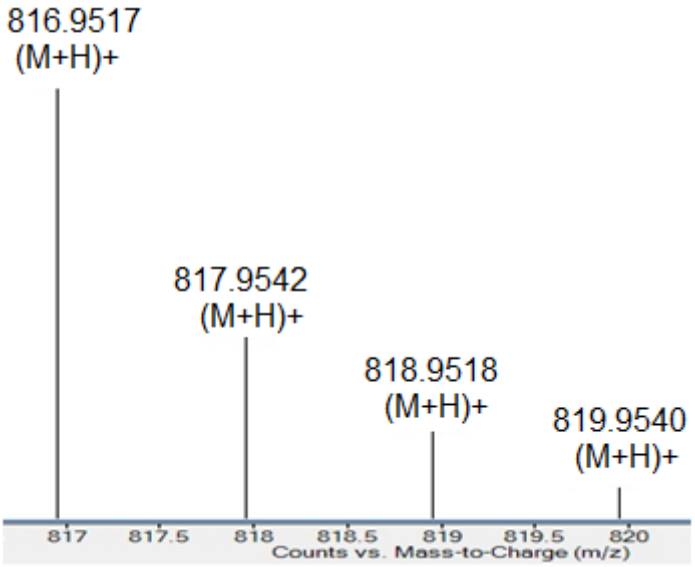

Fig. S8 ESI-MS experimental (bottom) and theoretical (top) isotopic distribution patterns of $[\{(CO)_3Mn(\mu\text{-}SC_6H_5)_2Mn(CO)_3\}(\mu\text{-pdi})]$ (**2**): $[M+H]^+$.

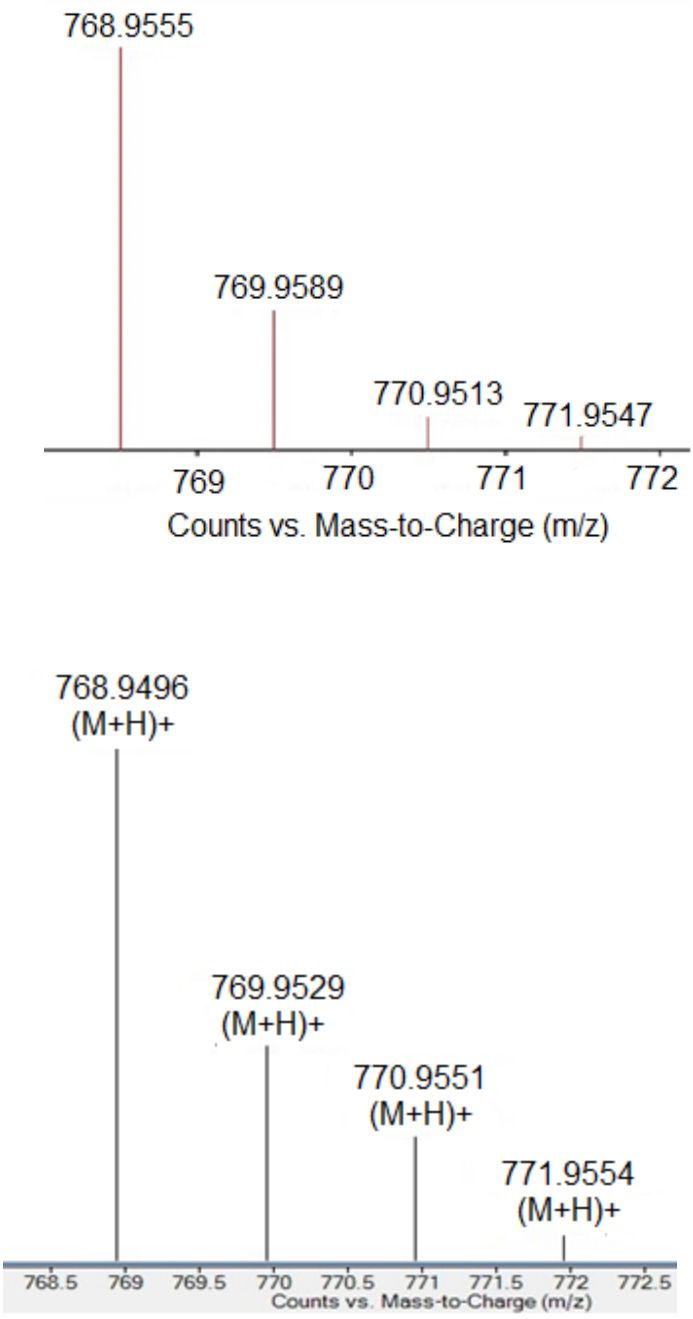

Fig. S9 ESI-MS experimental (bottom) and theoretical (top) isotopic distribution patterns of $[\{(CO)_3Mn(\mu\text{-}SC_6H_5)_2Mn(CO)_3\}(\mu\text{-edp})]$ (**3**): $[M+H]^+$.

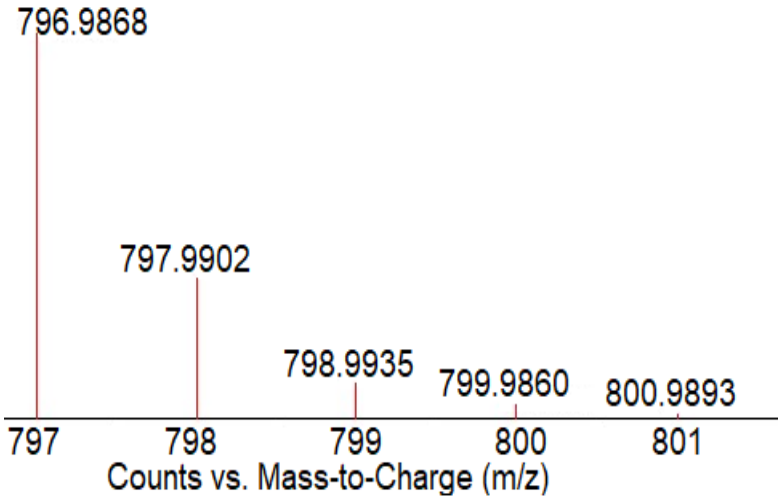

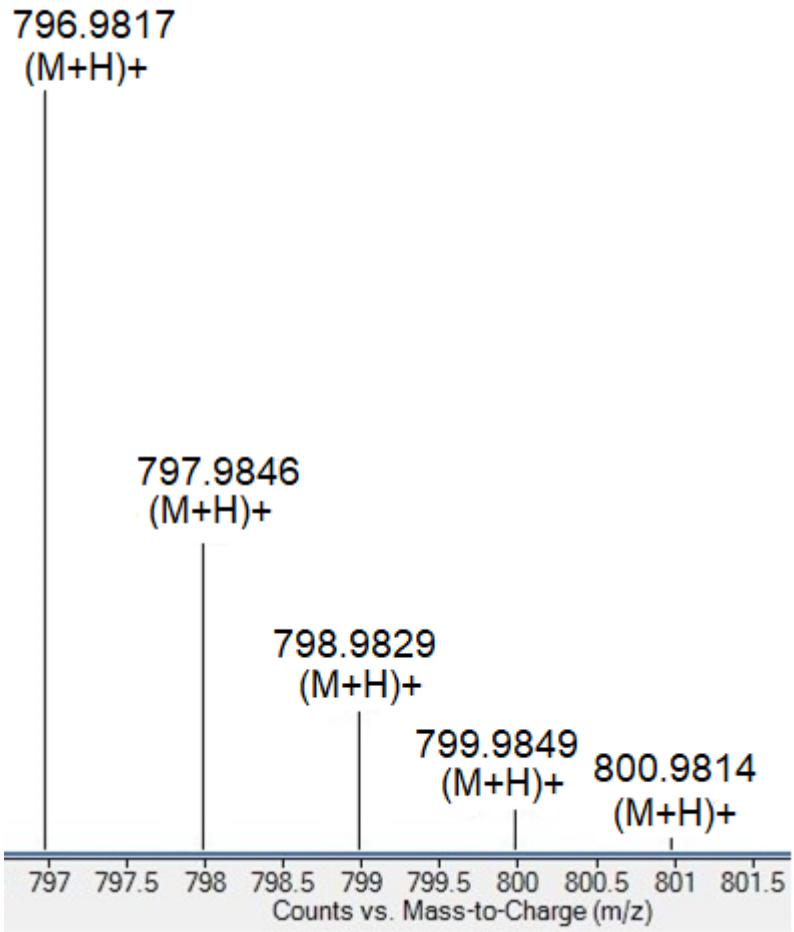

Fig. S10 ESI-MS experimental (bottom) and theoretical (top) isotopic distribution patterns of $[\{(CO)_3Mn(\mu\text{-}SC_6H_5)_2Mn(CO)_3\}(\mu\text{-bdp})]$ (**4**): $[M+H]^+$.

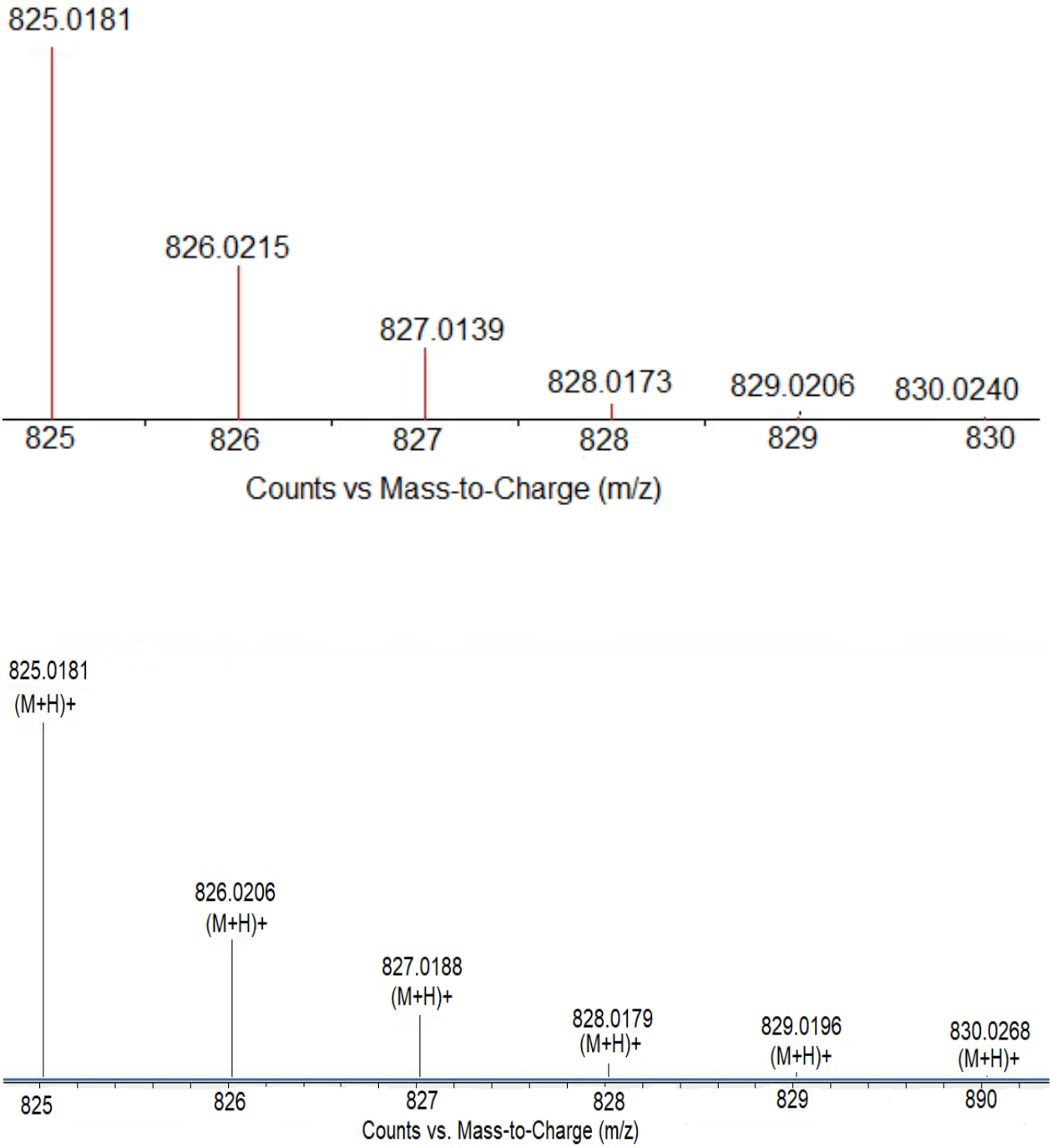

Fig. S11 ESI-MS experimental (bottom) and theoretical (top) isotopic distribution patterns of $[\{(CO)_3Mn(\mu\text{-}SC_6H_5)_2Mn(CO)_3\}(\mu\text{-hdp})]$ (**5**): $[M+H]^+$.

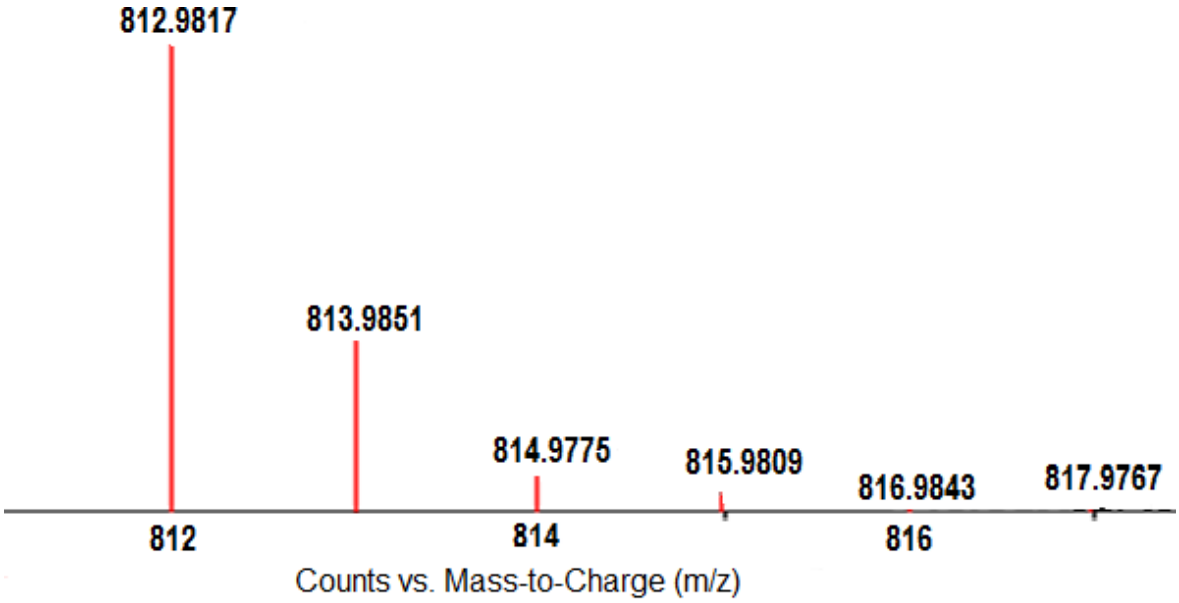

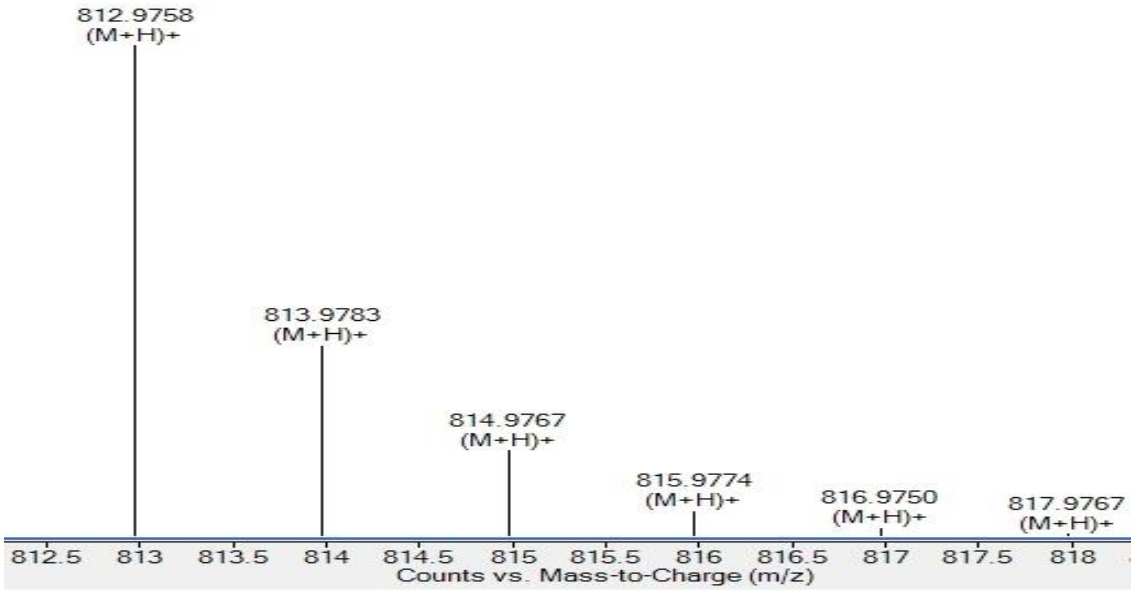

Fig. S12 ESI-MS experimental (bottom) and theoretical (top) isotopic distribution patterns of $[\{(CO)_3Mn(\mu\text{-}SC_6H_5)_2Mn(CO)_3\}(\mu\text{-pcadgd})]$ (**6**): $[M+H]^+$.

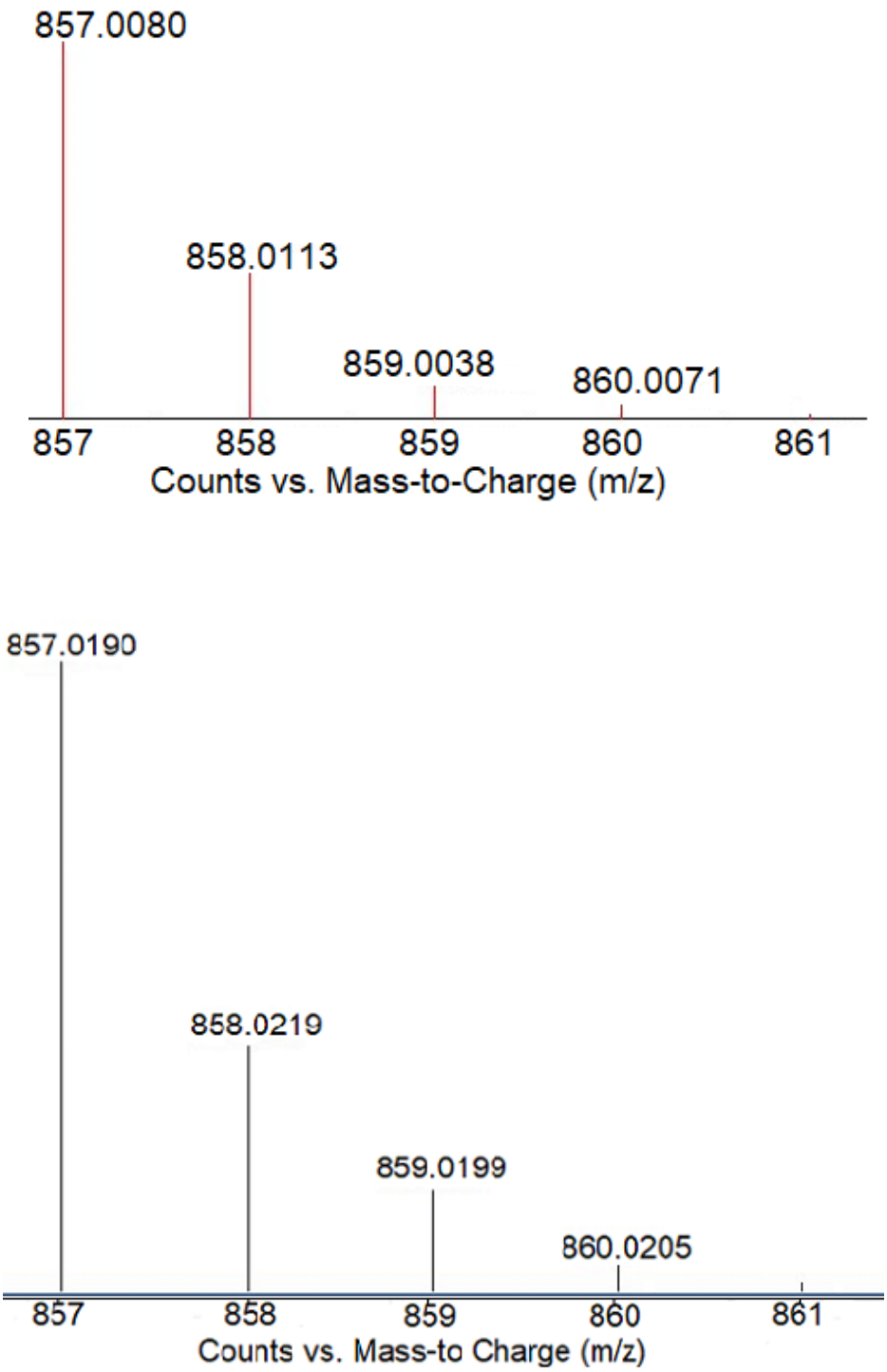

Fig. S13 ESI-MS experimental (bottom) and theoretical (top) isotopic distribution patterns of [{$(CO)_3Mn(\mu\text{-}SC_6H_5)_2Mn(CO)_3$}($\mu$-pcatgd)] (**7**): $[M+H]^+$.

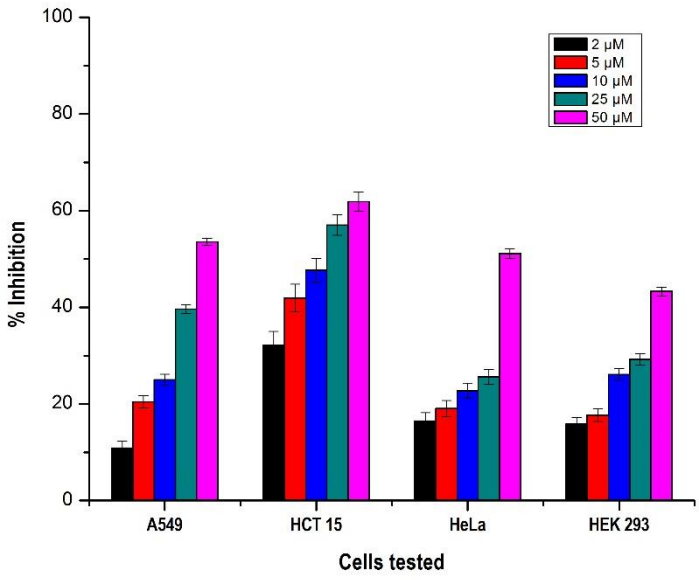

Fig. S14 Cytotoxic activities of different concentrations (2, 5, 10, 25, and 50 µM) of compound **1** in lung (A549), colon (HCT-15), and cervical (HeLa) cancer cells and normal human embryonic kidney (HEK 293) cells upon 48 h of treatment.

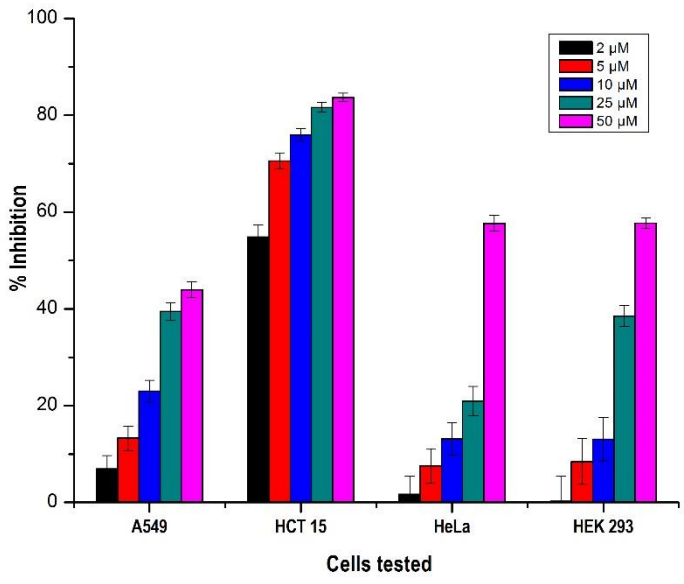

Fig. S15 Cytotoxic activities of different concentrations (2, 5, 10, 25, and 50 µM) of compound **2** in lung (A549), colon (HCT-15), and cervical (HeLa) cancer cells and normal human embryonic kidney (HEK 293) cells upon 48 h of treatment.

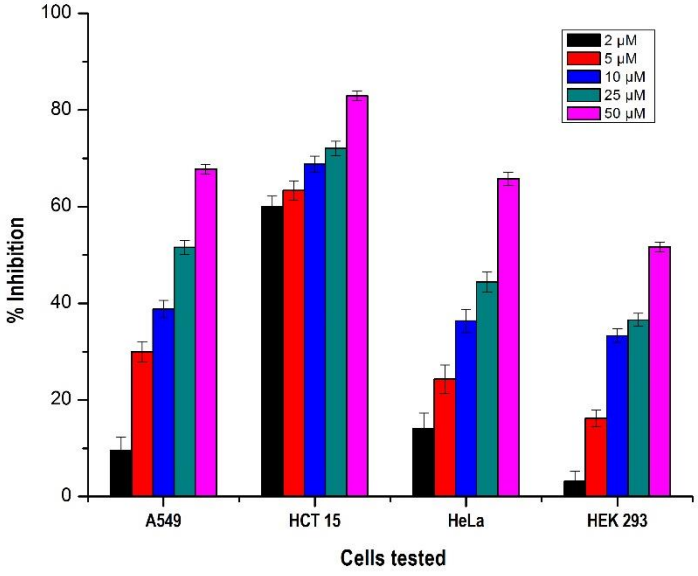

Fig. S16 Cytotoxic activities of different concentrations (2, 5, 10, 25, and 50 µM) of compound **4** in lung (A549), colon (HCT-15), and cervical (HeLa) cancer cells and normal human embryonic kidney (HEK 293) cells upon 48 h of treatment.

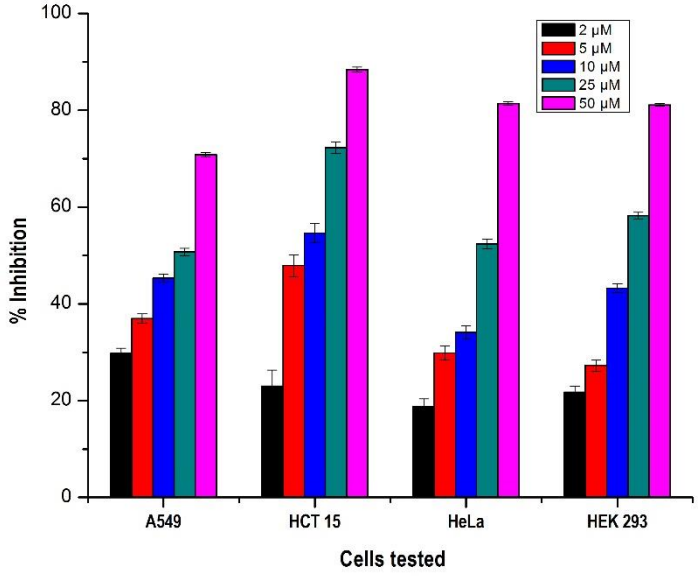

Fig. S17 Cytotoxic activities of different concentrations (2, 5, 10, 25, and 50 µM) of compound **5** in lung (A549), colon (HCT-15), and cervical (HeLa) cancer cells and normal human embryonic kidney (HEK 293) cells upon 48 h of treatment.

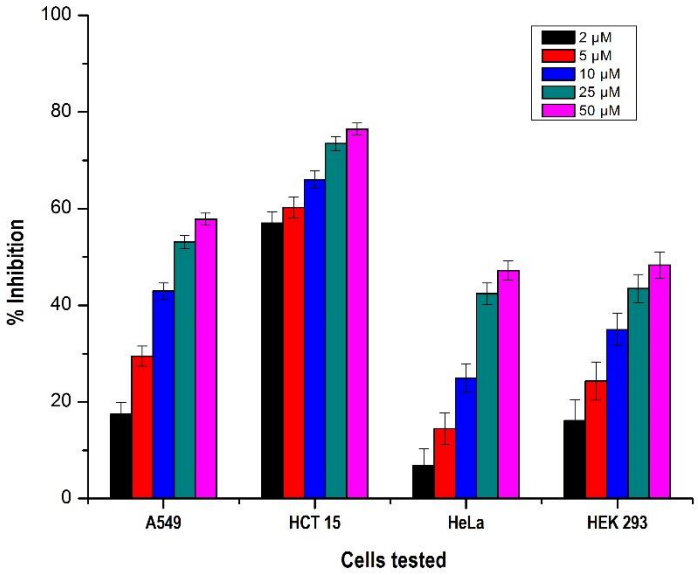

Fig. S18 Cytotoxic activities of different concentrations (2, 5, 10, 25, and 50 µM) of compound **6** in lung (A549), colon (HCT-15), and cervical (HeLa) cancer cells and normal human embryonic kidney (HEK 293) cells upon 48 h of treatment.

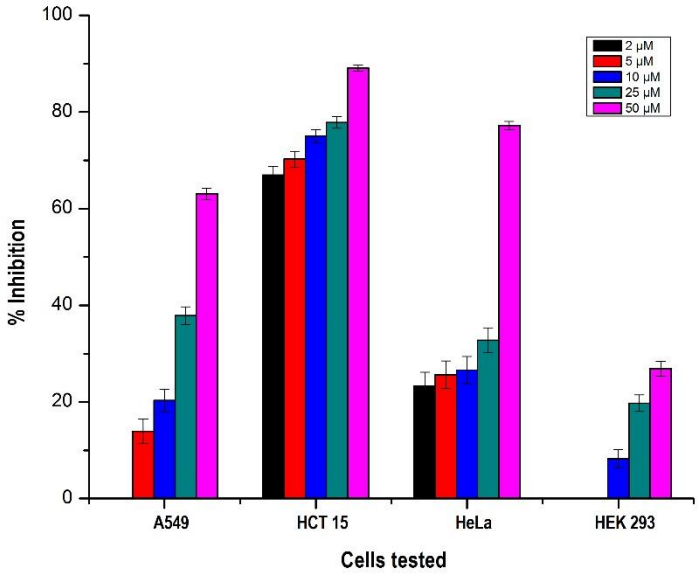

Fig. S19 Cytotoxic activities of different concentrations (2, 5, 10, 25, and 50 µM) of compound **7** in lung (A549), colon (HCT-15), and cervical (HeLa) cancer cells and normal human embryonic kidney (HEK 293) cells upon 48 h of treatment.

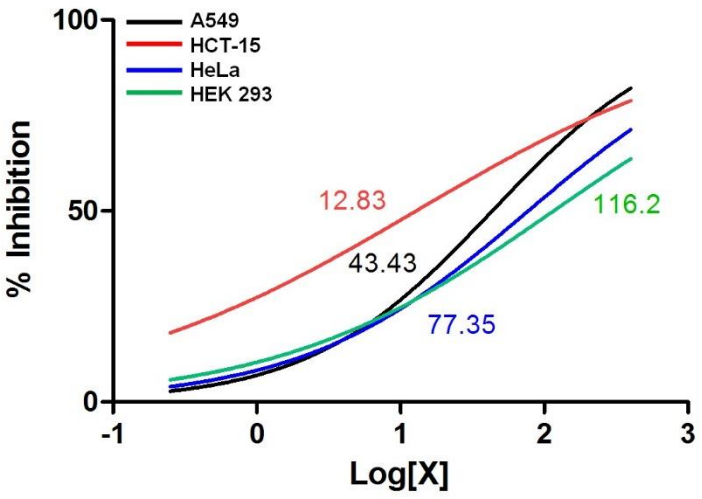

Fig. S20 Dose response curves showing sigmoidal model fit with the deduced IC_{50} values of compound **1** for lung (A549), colon (HCT-15), cervical (HeLa) and human embryonic kidney (HEK 293) cells.

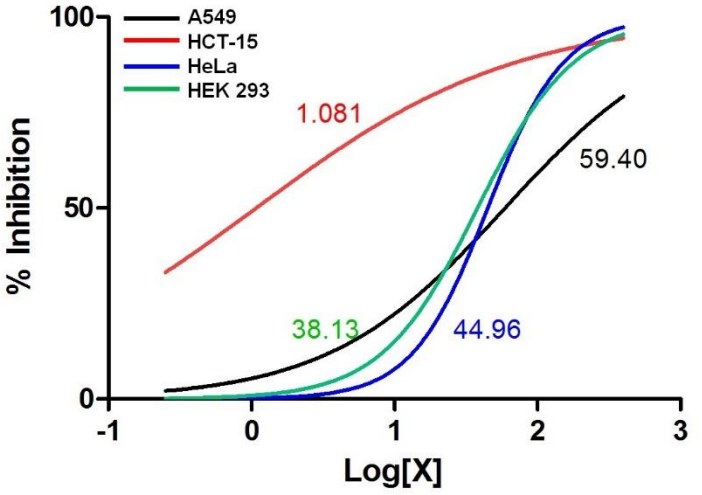

Fig. S21 Dose response curves showing sigmoidal model fit with the deduced IC_{50} values of compound **2** for lung (A549), colon (HCT-15), cervical (HeLa) and human embryonic kidney (HEK 293) cells.

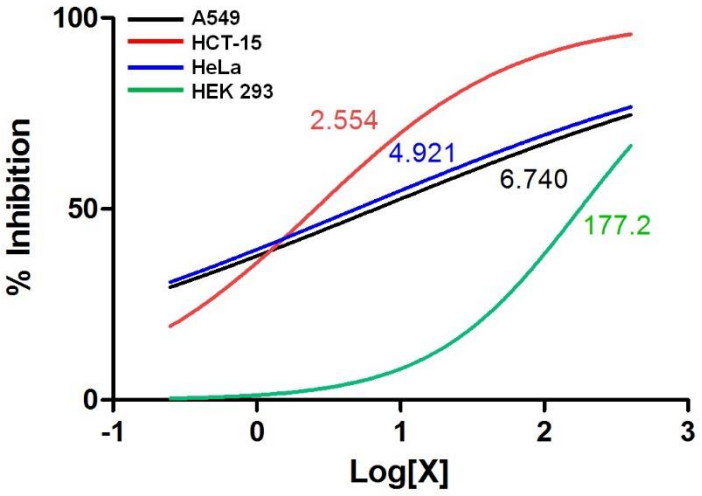

Fig. S22 Dose response curves showing sigmoidal model fit with the deduced IC_{50} values of compound **3** for lung (A549), colon (HCT-15), cervical (HeLa) and human embryonic kidney (HEK 293) cells.

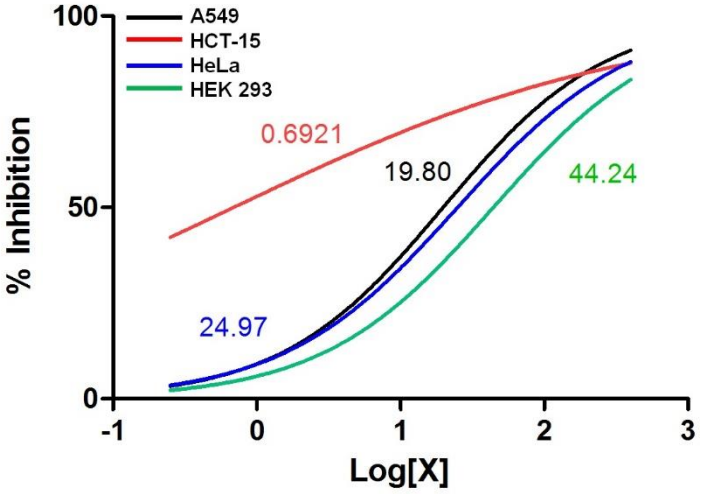

Fig. S23 Dose response curves showing sigmoidal model fit with the deduced IC_{50} values of compound **4** for lung (A549), colon (HCT-15), cervical (HeLa) and human embryonic kidney (HEK 293) cells.

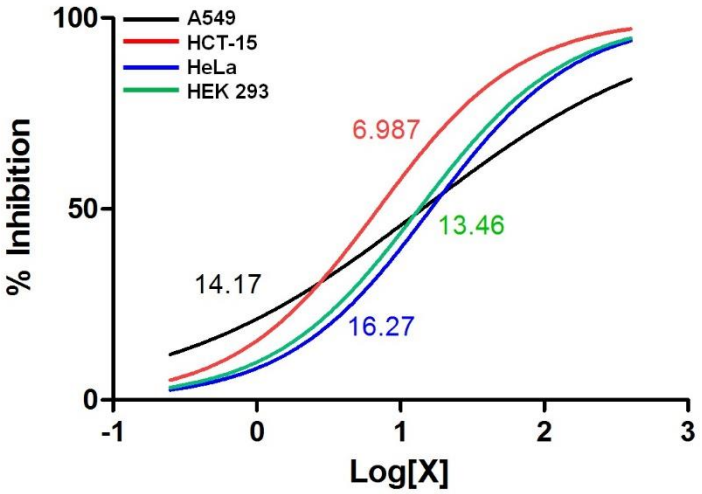

Fig. S24 Dose response curves showing sigmoidal model fit with the deduced IC_{50} values of compound **5** for lung (A549), colon (HCT-15), cervical (HeLa) and human embryonic kidney (HEK 293) cells.

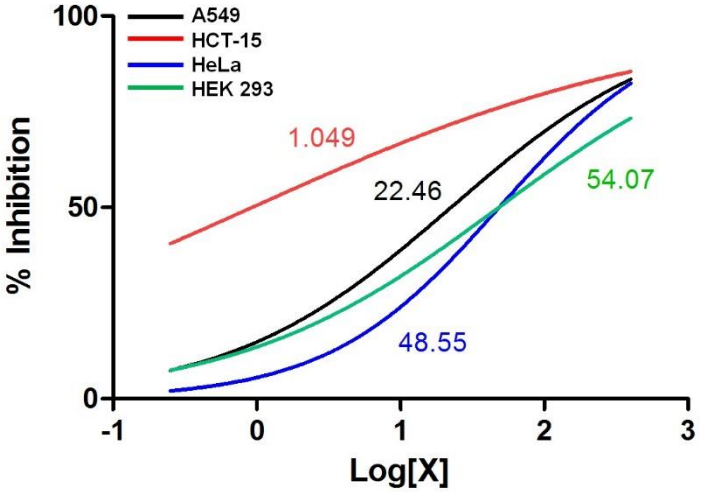

Fig. S25 Dose response curves showing sigmoidal model fit with the deduced IC_{50} values of compound **6** for lung (A549), colon (HCT-15), cervical (HeLa) and human embryonic kidney (HEK 293) cells.

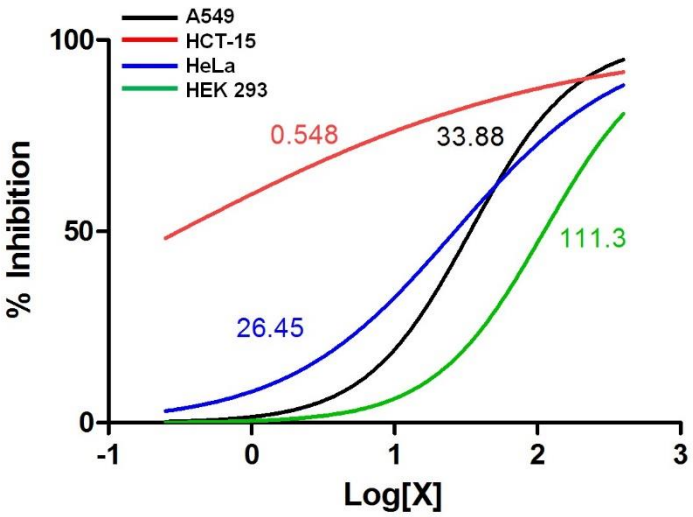

Fig. S26 Dose response curves showing sigmoidal model fit with the deduced IC_{50} values of compound **7** for lung (A549), colon (HCT-15), cervical (HeLa) and human embryonic kidney (HEK 293) cells.